Measurement-Induced Lévy Flights of Quantum Information

Igor Poboiko,[1,2,*] Marcin Szyniszewski,[3,4,*] Christopher J. Turner,[3] Igor V. Gornyi,[1,2]
Alexander D. Mirlin,[1,2] and Arijeet Pal[3]

[1]Institute for Quantum Materials and Technologies, Karlsruhe Institute of Technology, 76131 Karlsruhe, Germany
[2]Institut für Theorie der Kondensierten Materie, Karlsruhe Institute of Technology, 76131 Karlsruhe, Germany
[3]Department of Physics and Astronomy, University College London, Gower Street, London, WC1E 6BT, United Kingdom
[4]Department of Computer Science, University of Oxford, 15 Parks Road, Oxford OX1 3QD, United Kingdom

(Received 22 January 2025; revised 17 April 2025; accepted 30 September 2025; published 21 October 2025)

We explore a model of free fermions in one dimension, subject to *frustrated* (noncommuting) local measurements across adjacent sites, which resolves the fermions into nonorthogonal orbitals, misaligned from the underlying lattice. For maximal misalignment, superdiffusive behavior emerges from the vanishing of the measurement-induced quasiparticle decay rate at one point in the Brillouin zone, which generates fractal-scaling entanglement entropy $S \propto \ell^{1/3}$ for a subsystem of length ℓ. We derive an effective nonlinear sigma model with long-range couplings responsible for Lévy flights in entanglement propagation, which we confirm with large-scale numerical simulations. When the misalignment is reduced, the entanglement exhibits, with increasing ℓ, consecutive regimes of superdiffusive, $S \propto \ell^{1/3}$, diffusive, $S \propto \ln \ell$, and localized, $S = \text{const}$, behavior. Our findings show how intricate fractal-scaling entanglement can be produced for local Hamiltonians and measurements.

DOI: 10.1103/tx71-1cd9

Introduction—Quantum dynamics in many-body systems subjected to measurements has attracted much attention. It was, in particular, shown that quantum measurements may induce transitions between phases with the different scaling of entanglement entropy S as a function of subsystem size ℓ [1–7] (see also reviews on monitored quantum circuits [8,9]). A special role in this context is played by systems of free complex fermions with local density measurements preserving the Gaussian character of the state [4,10–20]. It was shown that in one-dimensional (1D) geometry, $S(\ell)$ saturates as $\ell \to \infty$ (area law) [15,20] (cf. Refs. [4,12]). For small measurement rate γ, it is preceded by an intermediate range of ℓ with the scaling $S \sim \gamma^{-1} \ln \ell$. In $d > 1$ dimensions, a measurement-induced transition between an area-law phase and a phase with $\ell^{d-1} \ln \ell$ scaling of S is found [16,17]. There is a remarkable relation between the physics of monitored systems in d dimensions and Anderson localization in disordered systems in $d+1$ dimensions, with the area law for $S(\ell)$ corresponding to the localized phase and the $S \propto \ell^{d-1} \ln \ell$ behavior to the diffusive phase (or diffusive regime for $d = 1$). This relation can be inferred from the comparison of the respective field theories—nonlinear sigma models (NLSMs)—for the two problems [15–17,19–25].

Importantly, local measurements on free fermions prevent establishing a volume-law phase ($S \propto \ell^d$) [26], which is a typical phase in generic weakly monitored quantum circuits. The appearance of the volume-law phase for fermions requires interactions between particles [23,24], which breaks down the Gaussianity of the many-body states. Even more tricky is to obtain a *fractal* subextensive scaling of entanglement ($S \propto \ell^\zeta$ with $d-1 < \zeta < d$) in monitored systems, although it was reported for, e.g., space-time dual quantum circuits [27], long-range interacting Hamiltonians or unitary gates [28–30], or "long-range dissipation and monitoring" [31,32]. In this context, noncommutativity ("frustration") of measurement operators (among themselves or with respect to the unitary dynamics of the system [7,18,22,30,33–35]) is expected to be of crucial importance for the phase diagrams. Another interesting class of models is based on the measurement-only dynamics [35–37], where the quasilocal, possibly noncommuting measurements give rise to both generation and suppression of entanglement.

In this Letter, we explore a 1D model of monitored free fermions, with the measurement operator being a particle number in a state residing on two adjacent sites (rather than on a single site), Fig. 1. This extension affects neither the U(1) symmetry (particle-number onservation) nor the local character of the measurement operator, nor the Gaussianity of the states. In view of the universality of diffusion and

*These authors contributed equally to this work.

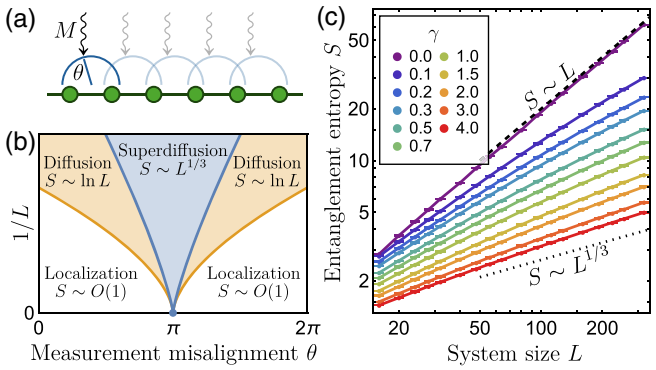

FIG. 1. (a) Model: free-fermion chain of size L continuously monitored via frustrated measurements with a misalignment θ. (b) "Phase diagram" of this system showing superdiffusion at $\theta = \pi$, with characteristic regimes of the entanglement scaling indicated by different colors. (c) Half-chain entanglement entropy S as a function of L for different values of the measurement strength γ at fixed $\theta = \pi$. The dashed line shows the extensive ("ballistic") behavior $S \sim L$, while the dotted line shows the fractal scaling $S \sim L^{1/3}$ corresponding to superdiffusion in $1+1$-dimensional space-time.

localization for given symmetry class and spatial dimensions, one could thus expect that the model belongs to the same "universality class" as previously studied 1D fermionic models [15]. Remarkably, this is not always the case. We discover the emergence of the physics of superdiffusion (Lévy flights) of quantum information, with a fractal power-law scaling $S(\ell) \propto \ell^{1/3}$, which persists into the measurement-only limit. We emphasize that, at variance with previous works, such behavior is observed in an intrinsically short-ranged free-fermion model.

Model—We consider a model of monitored free fermions with noncommuting measurements and U(1) particle-number symmetry, on a periodic chain of L sites [Fig. 1(a)]. The monitored dynamics is characterized by the stochastic Schrödinger equation [4,38],

$$d|\psi_{t+dt}\rangle = \Big[-idtH - \frac{\gamma dt}{2}\sum_i (M_i - \langle M_i\rangle)^2 + \sum_i d\xi_i^t (M_i - \langle M_i\rangle)\Big]|\psi_t\rangle, \tag{1}$$

where γ is the measurement strength, and $d\xi_i^t$ is the Itô increment with variance γdt. The Hamiltonian includes fermion hopping, $H = J\sum_i c_{i+1}^\dagger c_i + \text{H.c.}$, where J is the hopping strength. This stochastic evolution describes continuous monitoring of M_i [38], which we define to be the following two-site operator:

$$M_i = d_i^\dagger d_i, \qquad d_i = c_i \cos\frac{\theta}{4} + c_{i+1}\sin\frac{\theta}{4}, \tag{2}$$

where parameter θ can be interpreted as a misalignment of the measurement apparatus that causes a superposition of two adjacent sites to be measured. When this misalignment is nonzero, the measurement operators on adjacent bonds do not commute, leading to frustration in the chain, with the maximal frustration happening for $\theta = \pi$.

This continuous monitoring can be realized through weak interaction of every pair of adjacent sites with its ancilla [39–41]; the latter is then projectively measured with a period dt. Note that the specific sequence of measurements within the time interval dt becomes immaterial in the continuous-time limit $dt \to 0$. Since this evolution preserves the Gaussianity of the state, it is computationally simulable in polynomial time, and any state properties can be calculated from the corresponding single-particle correlation matrix $\mathcal{G}_{ij} = \langle c_i^\dagger c_j\rangle$. In detail, we use the algorithm of Refs. [4,10,14,42], where the state is represented as an $N \times L$ matrix ($N = L/2$ being the number of particles), and the evolution involves multiplication by $L \times L$ matrices corresponding to H and M_i, see Supplemental Material (SM) [43].

Judging from the previous analytical description of monitored free fermions with the U(1) symmetry [15], one would be tempted to conclude that at a large enough spatial scale, this model should exhibit localization (i.e., area-law entanglement), with an intermediate logarithmic regime at small γ. However, a numerical analysis of the entanglement entropy at $\theta = \pi$ in Fig. 1(c) (where $\ell = L/2$) indicates the absence of localization, even at large measurement strengths. Furthermore, the data surprisingly reveal an entanglement growth that is faster than logarithmic. As we demonstrate analytically later, and support by a thorough numerical analysis, the entropy grows as $S \propto \ell^{1/3}$, which corresponds to a superdiffusive transport in $1+1$ (space-time) dimensions.

Note that measurement operators similar to Eq. (2) were employed in a model of monitored Majorana fermions [21,22,35,48,49], which violates the U(1) symmetry: there, a superposition of Majorana operators at adjacent sites was considered. The physics in these works is related to logarithmic antilocalization quantum corrections in symmetry classes D and DIII. This is very different from Lévy-flight-induced superdiffusion of quantum information leading to the power-law fractal scaling of entanglement entropy studied here.

Effective field theory—Our analytical description of the problem is based on the replicated Keldysh NLSM approach, developed in Refs. [15,16,24] and extended to weak measurements in Ref. [17], see SM [43] for details. We introduce the Keldysh fermionic path-integral representation defined on $R \to 1$ replicas of the Keldysh contour. Averaging over the white noise $\xi(t)$ present in Eq. (1) leads to the quartic fermionic term in the action. This term is decoupled by means of the Hubbard-Stratonovich matrix-valued field $\hat{Q}(x,t)$, which is interpreted as the local equal-time Green's function of d fermions, $Q_{\alpha\beta}(x,t) \sim 2\langle d_\alpha(x,t) d_\beta^*(x,t)\rangle$. Here, indices include the structure in the Keldysh and replica spaces,

$\alpha,\beta \in \{+,-\}_{\mathrm{K}} \otimes \{1,\ldots,R\}_{\mathrm{R}}$, and the spatial coordinate x is a continuous version of the lattice index i. The Goldstone manifold consists of a replica-symmetric sector, the two-dimensional sphere S^2, which describes the Lindbladian dynamics, and a replicon sector, the special unitary group $\hat{U} \in \mathrm{SU}(R)$, which describes the dynamics of observables that are nonlinear in the density matrix.

The crucial observation, which is responsible for the superdiffusive spreading of the quantum information in the system, is that the measurement-induced quasiparticle decay rate has the following momentum-dependent form:

$$\gamma_k = \gamma\left(1 + \sin\frac{\theta}{2}\cos k\right), \tag{3}$$

and vanishes at $k = \pm\pi$ for a special point $\theta = \pi$. It happens because, for $\theta = \pi$, the operator $d_i = (c_i + c_{i+1})/\sqrt{2}$ (and hence M_i) exactly nullifies the state with $k = \pm\pi$. Thus, such states are completely unaffected by measurements. Interestingly, this does not affect the diffusive behavior of the Lindbladian dynamics observed earlier [15] in the conventional density monitoring case $\theta = 0$. The spatial diffusion coefficient consists of two contributions attributed to the unitary dynamics and noncommutativity of measurements,

$$\begin{aligned} D &= \int_{-\pi}^{\pi} \frac{(dk)}{\gamma_k}\left[\left(\frac{\partial \xi_k}{\partial k}\right)^2 + \frac{1}{4}\left(\frac{\partial \gamma_k}{\partial k}\right)^2\right] \\ &= \frac{4J^2}{\gamma}\frac{1}{1+\left|\cos\frac{\theta}{2}\right|} + \frac{\gamma}{4}\left(1 - \left|\cos\frac{\theta}{2}\right|\right), \end{aligned} \tag{4}$$

and remains finite at $\theta = \pi$, since both the group velocity $\xi_k' = -2J\sin k$ and the derivative γ_k' vanish at $k = \pm\pi$ similar to γ_k.

We now focus on the replicon sector, which describes observables of our interest. To see the emergence of superdiffusion, we inspect the quadratic form of the action (see SM [43] for the full action of NLSM) in $1+1$ dimensions. In the spatial direction, it has a conventional diffusive form characterized by the diffusion coefficient D, Eq. (4). On the other hand, vanishing of γ_k leads to nonlocality of the temporal term in the action characterized by the diffusion kernel $\mathcal{B}(t_1 - t_2)$, with the Fourier transform given by

$$\begin{aligned} \mathcal{B}(\omega) &= \int_{-\pi}^{\pi} \frac{(dk)}{\gamma_k - i\omega} = \frac{1}{\sqrt{(\gamma - i\omega)^2 - \gamma^2 \sin^2\frac{\theta}{2}}} \\ &\overset{\omega\to 0}{\approx} \begin{cases} \left(\gamma\left|\cos\frac{\theta}{2}\right|\right)^{-1}, & \theta \neq \pi, \\ [-2i\gamma(\omega + i0)]^{-1/2}, & \theta = \pi. \end{cases} \end{aligned} \tag{5}$$

The emergence of superdiffusive Lévy flights with exponent $\alpha = 3/2$—resulting in a heavy-tailed distribution of quantum-information spreading—in our theory at $\theta = \pi$ is manifest in the last line of Eq. (5). The physics behind superdiffusion at $\theta = \pi$ is as follows. The states with k close to $\pm\pi$ are nearly eigenstates of measurement operators M_i and thus propagate ballistically for long times $\sim 1/\gamma_k$ [see Eq. (3)] before they get substantially affected by measurements that limit quantum correlations.

The superdiffusive character of the field theory leads to the fractal scaling of observables. We focus below on the entanglement entropy (for a subsystem A of length ℓ) $S_A = -\overline{\mathrm{Tr}(\hat{\rho}_A \ln \hat{\rho}_A)}$ and the charge correlation function

$$C(x - x') = \overline{\langle \hat{n}(x)\hat{n}(x')\rangle - \langle \hat{n}(x)\rangle\langle \hat{n}(x')\rangle}, \tag{6}$$

where the overbar denotes averaging over quantum trajectories. Let us emphasize that $C(x - x')$ is a fundamental characteristic of the system, which governs the scaling of various key observables. In particular, it determines the second cumulant of charge $\mathcal{C}_A^{(2)}$,

$$\mathcal{C}_A^{(2)} = \overline{\langle \hat{N}_A^2\rangle - \langle \hat{N}_A\rangle^2} = \int_0^{\ell} dx dx' C(x - x'), \tag{7}$$

which, in view of the Gaussian character of the state, is related to the entropy via

$$S_A \approx (\pi^2/3)\mathcal{C}_A^{(2)}. \tag{8}$$

The exact relation [50] also contains terms proportional to higher cumulants. However, they do not affect the scaling and amount to a small correction only, as was found for conventional density monitoring [15]; we have also verified this for the present model [43]. Both the entropy and the charge-cumulant generating function can be expressed via the NLSM partition function with appropriate boundary conditions [24,43].

Fractality of correlations and entanglement—We first consider the problem within the quasiclassical approximation with the Gaussian action. For $\delta = \theta - \pi \ll 1$, the Fourier transform of Eq. (6) reads

$$C(q) \approx \begin{cases} (2|\delta|)^{-1/2}|q\ell_0|, & q\ell_0 \ll |\delta|^{3/2}, \\ (2^{-2/3}3^{-1/2})|q\ell_0|^{2/3}, & |\delta|^{3/2} \ll q\ell_0 \ll 1, \\ \mathrm{const}, & 1 \lesssim q\ell_0, \end{cases} \tag{9}$$

where $\ell_0 = \sqrt{D/\gamma} \approx \sqrt{(2J/\gamma)^2 + 1/4}$ is the mean free path. Thus, $\delta = 0$ ($\theta = \pi$) is a critical point, where $C(q) \propto q^{2/3}$ for $q\ell_0 \to 0$, and the system exhibits a fractal (superdiffusive) scaling of the charge cumulant and entropy,

$$S_A \sim \mathcal{C}_A^{(2)} \sim \ell_0(L/\ell_0)^{1/3} \quad \text{for } \ell = L/2 \gg \ell_0, \tag{10}$$

explaining the surprising numerical results from Fig. 1. At small measurement strength γ, the entropy for small system

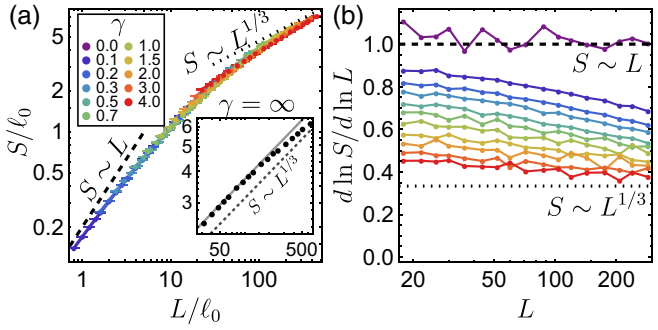

FIG. 2. (a) Collapse of S/ℓ_0, where S is half-chain entanglement entropy, as a function of L/ℓ_0 for $\theta = \pi$ and measurement rates from $\gamma = 0$ to $\gamma = 4$. The inset shows results for $\gamma = \infty$, which are of the form $S = s(L)L^{1/3}$, where $s(L)$ exhibits a slow crossover from a finite value at $L \sim 30\ell_0$ to a slightly smaller finite value at $L \to \infty$ due to quantum corrections, see SM [43]. (b) $d \ln S/d \ln L$ as a function of the system size. Legend in (a) applies in (b). The dashed lines show the ballistic behavior $S \sim L$, while the dotted lines show superdiffusion $S \sim L^{1/3}$ in the thermodynamic limit.

sizes scales extensively with the system size $S \sim L$, which then experiences a ballistic-to-superdiffusion crossover, corresponding to the crossover between the second and third lines of Eq. (9), as one increases L or γ. This change in the entanglement behavior can be seen in Fig. 2(a), where we observe a nearly perfect data collapse of S/ℓ_0 vs L/ℓ_0 in a broad range of γ, from 0.1 to 4.0. Analytically, this universality of the crossover function is, strictly speaking, derived for $\gamma \ll 1$, in view of numerical corrections to the prefactor of $L^{1/3}$ scaling at $\gamma \gtrsim 1$, which come from spatial scales of the order of the lattice spacing and are not included in the NLSM analysis. We see, however, from Fig. 2(a) that the universality holds excellently up to a large measurement rate, $\gamma = 4$. This universality shows that quantum corrections are essentially irrelevant even for rather large γ. A similar theory, with diffusive transport along one axis and superdiffusive along the other axis, was derived for transport in graphene with anisotropic disorder [51]. It was found there that quantum localization amounts to a finite correction only, without inducing strong localization or a localization transition. The ballistic-to-superdiffusion crossover is further demonstrated in Fig. 2(b), where the logarithmic derivative $d \ln S/d \ln L$ is shown to approach the $1/3$ asymptotic value in the large-L limit, $L/\ell_0 \to \infty$. Our conclusions are additionally supported by an analysis of finite-size corrections to the superdiffusive scaling in SM [43].

Remarkably, the superdiffusive behavior and the absence of localization also hold in the measurement-only case, $\gamma = \infty$, see inset of Fig. 2(a), in agreement with the analytical results. At the same time, the $\gamma = \infty$ data slightly deviate (bend down) from the universal scaling curve. This has two reasons. First, for $\gamma = \infty$, quantum corrections to the prefactor of the $L^{1/3}$ scaling mentioned in the preceding paragraph are particularly pronounced. Second, the $\gamma = \infty$ model belongs to a different symmetry class, as we are going to explain. A free-fermion system with particle-number conservation belongs to the BDI symmetry class when the Hamiltonian exhibits a particle-hole symmetry $H = -H^T$ and, in the same basis, the measurement operators are real $M = M^*$; otherwise, it belongs to the AIII class [20,24]. For any finite γ, our model is therefore in the AIII class, while, for $\gamma = \infty$, the Hamiltonian is absent in the stochastic Schrödinger equation and the measurement-only point has a larger BDI symmetry. The difference between the NLSM field theories of these two classes is minimal and does not affect the qualitative behavior. The one-loop weak-localization correction in class BDI is negative and twice larger than that for class AIII. In our model, this is expected to lead to a numerical reduction of the prefactor s of $S = sL^{1/3}$ scaling in the $\gamma = \infty$ case (BDI class). This is what is observed in our simulations [inset of Fig. 2(a)]: $s(L)$ slowly interpolates between two finite values, as expected from the weak-localization correction, see SM [43].

For a nonzero (but small) δ, the system exhibits a crossover from superdiffusive regime $C(q) \propto q^{2/3}$ to diffusive regime $C(q) \propto q$ at momentum $q\ell_0 \sim |\delta|^{3/2}$, which corresponds to a length scale $\ell^* \sim \ell_0 |\delta|^{-3/2}$. Ultimately, at large system sizes, the system then crosses over into localization, $C(q)/q \to 0$. We confirm this behavior using finite-size numerics in Fig. 3(a), where we plot the ratio $C(q)/q$. The three distinct regimes are clearly observed: superdiffusion (dashed line), diffusion (approximate saturation, with a slow decrease towards small q due to weak-localization correction), and localization [vanishing $C(q)/q \propto q$ at $q \to 0$]. Translating to the real space, this implies that, as the system size is increased, one will first see the fractal (superdiffusive) entropy scaling $S \propto L^{1/3}$, then the logarithmic (diffusive) law $S \propto \ln L$, and finally the area law (localization) $S \simeq$ const, see Fig. 1(b).

In the diffusive regime, one can calculate the effective coupling constant (discarding localization effects),

$$g = \left.\frac{C(q)}{q}\right|_{q\ell^* \ll 1} \simeq \frac{\ell_0}{\sqrt{2}} |\delta|^{-1/2}. \tag{11}$$

This allows us to estimate the localization length, which scales at $|\delta| \ll 1$ as

$$\ell_{\rm loc} \sim \ell^* \exp(4\pi g) \simeq \ell_0 |\delta|^{-3/2} \exp \frac{2\sqrt{2}\pi \ell_0}{\sqrt{|\delta|}}. \tag{12}$$

The localization length $\ell_{\rm loc}(\delta)$ thus diverges exponentially at the critical point $\delta = 0$. If one fits Eq. (12) to a power-law form $\ell_{\rm loc} \sim |\delta|^{-\nu}$ in a restricted range of δ, one will get an "effective exponent" ν that increases from $3/2$ towards infinity when one approaches the singular point $\delta = 0$.

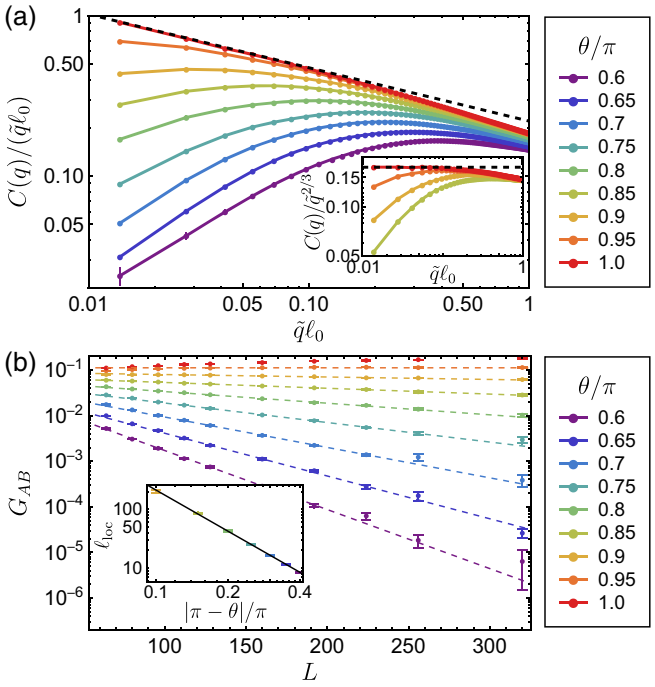

FIG. 3. (a) Correlation function $C(q)$ as a function of rescaled momentum $\tilde{q}\ell_0$, where $\tilde{q} = 2\sin(q/2)$ and $\ell_0 = \sqrt{(2J/\gamma)^2 + 1/4}$, for $\gamma = 4$ and different values of θ/π. The system size used is $L = 320$. The dashed line shows the superdiffusive behavior $C(q)/q \sim q^{-1/3}$. The inset shows $C(q)/q^{2/3}$, which saturates at $q \to 0$ for $\theta = \pi$. (b) Particle number covariance G_{AB} as a function of system size L for different values of θ/π. Dashed lines are fits to $\sim \exp(-L/4\ell_{\rm loc})$ for $L \geq 128$. The extracted localization length is shown in the inset, along with a power-law fit $\ell_{\rm loc} \sim |1-\theta/\pi|^{\nu}$, with exponent $\nu \approx 2.33(3)$ consistent with the analytical asymptotics (12) at numerically accessible scales.

To probe the localization in real space numerically, we use the particle-number covariance, $G_{AB} = \overline{\langle N_A\rangle\langle N_B\rangle - \langle N_A N_B\rangle}$, where N_A and N_B are particle-number operators of antipodal regions A and B, each of size $L/4$. This observable yields an effective conductance at scale $\sim L/4$ and scales in the area-law phase asymptotically as $G_{AB} \sim \exp(-L/4\ell_{\rm loc})$. Numerical results for $G_{AB}(L)$ shown in Fig. 3(b) confirm that localization sets in when $\theta \neq \pi$. By fitting $G_{AB}(L)$ to the exponential law for $L \geq 128$ (dashed lines), we obtain estimates for the localization length $\ell_{\rm loc}(\delta)$ shown in the inset. The results clearly support the analytically predicted divergence of $\ell_{\rm loc}$ at $\delta \to 0$. Accurately verifying Eq. (12) in this way is hardly possible since $\ell_{\rm loc}$ quickly becomes very large at small δ, where this formula holds. Instead, we show in the inset a power-law fit $\ell_{\rm loc} \sim |\delta|^{-\nu}$, which yields effective exponent $\nu \approx 2.33(3)$, which is larger than $3/2$ in agreement with a discussion below Eq. (12). Note that this effective exponent is not too far from $3/2$, which reflects the difficulty in numerical verification of the exponential dependence in Eq. (12): when the exponential decay of $G_{AB}(L)$ is observed for realistic system sizes, the localization length is only a few times larger than $\ell^* \sim \ell_0|\delta|^{-3/2}$.

Discussion and outlook—Summarizing, the free-fermion model with two-site monitoring operators (2) is characterized, at $\theta = \pi$, by a superdiffusive NLSM, which leads to the fractal scaling of the entanglement entropy, $S \propto L^{1/3}$, and charge correlations, $C(q) \propto q^{2/3}$. When θ deviates from the critical point π, the superdiffusive scaling is transient, giving rise to diffusion and, eventually, localization at longer length scales (smaller q). The superdiffusive behavior originates from the vanishing of the measurement-induced quasiparticle decay rate γ_k at one point in the Brillouin zone and should also hold for other models of monitoring having this property (also for other symmetry classes). An example is a model with measurement of conventional site density $c_i^\dagger c_i$ but on even sites only. A related mechanism of Lévy flights was found to be operative in nonmonitored models with "nodal" disorder [51,52], dephasing [53], and interactions [54]. Our discovery of measurement-induced Lévy flights opens up avenues for the study of exotic entangled phases and novel quantum-information transport mechanisms, including tailoring the entanglement growth in free-fermion monitored systems.

Acknowledgments—A. P. and M. S. were funded by the European Research Council (ERC) under the European Union's Horizon 2020 research and innovation programme (Grant Agreement No. 853368). M. S. was also supported by the Engineering and Physical Sciences Research Council grant on Robust and Reliable Quantum Computing (RoaRQ), Investigation 004 [Grant Reference No. EP/W032635/1]. C. J. T. is supported by an EPSRC fellowship (Grant Ref. No. EP/W005743/1). I. P. and A. D. M. acknowledge support by the Deutsche Forschungsgemeinschaft (DFG, German Research Foundation)—553096561. The authors acknowledge the use of the UCL High Performance Computing Facilities (Myriad), and associated support services, in the completion of this work.

Data availability—The data that support the findings of this article are openly available [55].

[1] Y. Li, X. Chen, and M. P. A. Fisher, Quantum Zeno effect and the many-body entanglement transition, Phys. Rev. B **98**, 205136 (2018).
[2] B. Skinner, J. Ruhman, and A. Nahum, Measurement-induced phase transitions in the dynamics of entanglement, Phys. Rev. X **9**, 031009 (2019).
[3] A. Chan, R. M. Nandkishore, M. Pretko, and G. Smith, Unitary-projective entanglement dynamics, Phys. Rev. B **99**, 224307 (2019).

[4] X. Cao, A. Tilloy, and A. De Luca, Entanglement in a fermion chain under continuous monitoring, SciPost Phys. **7**, 024 (2019).

[5] M. Szyniszewski, A. Romito, and H. Schomerus, Entanglement transition from variable-strength weak measurements, Phys. Rev. B **100**, 064204 (2019).

[6] Y. Li, X. Chen, and M. P. A. Fisher, Measurement-driven entanglement transition in hybrid quantum circuits, Phys. Rev. B **100**, 134306 (2019).

[7] Y. Bao, S. Choi, and E. Altman, Theory of the phase transition in random unitary circuits with measurements, Phys. Rev. B **101**, 104301 (2020).

[8] A. C. Potter and R. Vasseur, Entanglement dynamics in hybrid quantum circuits, in *Entanglement in Spin Chains: From Theory to Quantum Technology Applications*, edited by A. Bayat, S. Bose, and H. Johannesson (Springer International Publishing, Cham, 2022), pp. 211–249.

[9] M. P. Fisher, V. Khemani, A. Nahum, and S. Vijay, Random quantum circuits, Annu. Rev. Condens. Matter Phys. **14**, 335 (2023).

[10] O. Alberton, M. Buchhold, and S. Diehl, Entanglement transition in a monitored free-fermion chain: From extended criticality to area law, Phys. Rev. Lett. **126**, 170602 (2021).

[11] M. Buchhold, Y. Minoguchi, A. Altland, and S. Diehl, Effective theory for the measurement-induced phase transition of Dirac fermions, Phys. Rev. X **11**, 041004 (2021).

[12] M. Coppola, E. Tirrito, D. Karevski, and M. Collura, Growth of entanglement entropy under local projective measurements, Phys. Rev. B **105**, 094303 (2022).

[13] F. Carollo and V. Alba, Entangled multiplets and spreading of quantum correlations in a continuously monitored tight-binding chain, Phys. Rev. B **106**, L220304 (2022).

[14] M. Szyniszewski, O. Lunt, and A. Pal, Disordered monitored free fermions, Phys. Rev. B **108**, 165126 (2023).

[15] I. Poboiko, P. Pöpperl, I. V. Gornyi, and A. D. Mirlin, Theory of free fermions under random projective measurements, Phys. Rev. X **13**, 041046 (2023).

[16] I. Poboiko, I. V. Gornyi, and A. D. Mirlin, Measurement-induced phase transition for free fermions above one dimension, Phys. Rev. Lett. **132**, 110403 (2024).

[17] K. Chahine and M. Buchhold, Entanglement phases, localization, and multifractality of monitored free fermions in two dimensions, Phys. Rev. B **110**, 054313 (2024).

[18] L. Lumia, E. Tirrito, R. Fazio, and M. Collura, Measurement-induced transitions beyond Gaussianity: A single particle description, Phys. Rev. Res. **6**, 023176 (2024).

[19] E. Starchl, M. H. Fischer, and L. M. Sieberer, Generalized Zeno effect and entanglement dynamics induced by fermion counting, PRX Quantum **6**, 030302 (2025).

[20] M. Fava, L. Piroli, D. Bernard, and A. Nahum, Monitored fermions with conserved $U(1)$ charge, Phys. Rev. Res. **6**, 043246 (2024).

[21] C.-M. Jian, H. Shapourian, B. Bauer, and A. W. W. Ludwig, Measurement-induced entanglement transitions in quantum circuits of non-interacting fermions: Born-rule versus forced measurements, arXiv:2302.09094.

[22] M. Fava, L. Piroli, T. Swann, D. Bernard, and A. Nahum, Nonlinear sigma models for monitored dynamics of free fermions, Phys. Rev. X **13**, 041045 (2023).

[23] H. Guo, M. S. Foster, C.-M. Jian, and A. W. W. Ludwig, Field theory of monitored interacting fermion dynamics with charge conservation, Phys. Rev. B **112**, 064304 (2025).

[24] I. Poboiko, P. Pöpperl, I. V. Gornyi, and A. D. Mirlin, Measurement-induced transitions for interacting fermions, Phys. Rev. B **111**, 024204 (2025).

[25] A. Tiutiakina, H. Lóio, G. Giachetti, J. D. Nardis, and A. D. Luca, Field theory for monitored Brownian SYK clusters, Quantum **9**, 1794 (2025).

[26] L. Fidkowski, J. Haah, and M. B. Hastings, How dynamical quantum memories forget, Quantum **5**, 382 (2021).

[27] M. Ippoliti, T. Rakovszky, and V. Khemani, Fractal, logarithmic, and volume-law entangled nonthermal steady states via spacetime duality, Phys. Rev. X **12**, 011045 (2022).

[28] M. Block, Y. Bao, S. Choi, E. Altman, and N. Y. Yao, Measurement-induced transition in long-range interacting quantum circuits, Phys. Rev. Lett. **128**, 010604 (2022).

[29] S. Sharma, X. Turkeshi, R. Fazio, and M. Dalmonte, Measurement-induced criticality in extended and long-range unitary circuits, SciPost Phys. Core **5**, 023 (2022).

[30] J. Richter, O. Lunt, and A. Pal, Transport and entanglement growth in long-range random Clifford circuits, Phys. Rev. Res. **5**, L012031 (2023).

[31] A. C. C. de Albornoz, D. C. Rose, and A. Pal, Entanglement transition and heterogeneity in long-range quadratic Lindbladians, Phys. Rev. B **109**, 214204 (2024).

[32] A. Russomanno, G. Piccitto, and D. Rossini, Entanglement transitions and quantum bifurcations under continuous long-range monitoring, Phys. Rev. B **108**, 104313 (2023).

[33] O. Lunt and A. Pal, Measurement-induced entanglement transitions in many-body localized systems, Phys. Rev. Res. **2**, 043072 (2020).

[34] M. Van Regemortel, Z.-P. Cian, A. Seif, H. Dehghani, and M. Hafezi, Entanglement entropy scaling transition under competing monitoring protocols, Phys. Rev. Lett. **126**, 123604 (2021).

[35] R. Nehra, A. Romito, and D. Meidan, Controlling measurement-induced phase transitions with tunable detector coupling, Quantum **9**, 1697 (2025).

[36] M. Ippoliti, M. J. Gullans, S. Gopalakrishnan, D. A. Huse, and V. Khemani, Entanglement phase transitions in measurement-only dynamics, Phys. Rev. X **11**, 011030 (2021).

[37] K. Klocke and M. Buchhold, Majorana loop models for measurement-only quantum circuits, Phys. Rev. X **13**, 041028 (2023).

[38] H. M. Wiseman and G. J. Milburn, *Quantum Measurement and Control* (Cambridge University Press, Cambridge, England, 2009).

[39] X. Turkeshi, A. Biella, R. Fazio, M. Dalmonte, and M. Schirò, Measurement-induced entanglement transitions in the quantum Ising chain: From infinite to zero clicks, Phys. Rev. B **103**, 224210 (2021).

[40] E. V. H. Doggen, Y. Gefen, I. V. Gornyi, A. D. Mirlin, and D. G. Polyakov, Generalized quantum measurements with matrix product states: Entanglement phase transition and clusterization, Phys. Rev. Res. **4**, 023146 (2022).

[41] E. V. H. Doggen, Y. Gefen, I. V. Gornyi, A. D. Mirlin, and D. G. Polyakov, Evolution of many-body systems under

ancilla quantum measurements, Phys. Rev. B **107**, 214203 (2023).
[42] M. Szyniszewski, Unscrambling of single-particle wave functions in systems localized through disorder and monitoring, Phys. Rev. B **110**, 024303 (2024).
[43] See Supplemental Material at http://link.aps.org/supplemental/10.1103/tx71-1cd9 for details of the theoretical analysis and computational approach, which includes Refs. [44–47].
[44] A. D. Mirlin, Y. V. Fyodorov, F.-M. Dittes, J. Quezada, and T. H. Seligman, Transition from localized to extended eigenstates in the ensemble of power-law random banded matrices, Phys. Rev. E **54**, 3221 (1996).
[45] E. Brezin, J. Zinn-Justin, and J. C. L. Guillou, Critical properties near σ dimensions for long-range interactions, J. Phys. A **9**, L119 (1976).
[46] A. Kuznetsov, On extrema of stable processes, Ann. Probab. **39**, 1027 (2011).
[47] P. Wölfle and R. N. Bhatt, Electron localization in anisotropic systems, Phys. Rev. B **30**, 3542 (1984).
[48] G. Kells, D. Meidan, and A. Romito, Topological transitions in weakly monitored free fermions, SciPost Phys. **14**, 031 (2023).
[49] J. Merritt and L. Fidkowski, Entanglement transitions with free fermions, Phys. Rev. B **107**, 064303 (2023).
[50] I. Klich and L. Levitov, Quantum noise as an entanglement meter, Phys. Rev. Lett. **102**, 100502 (2009).
[51] S. Gattenlöhner, I. V. Gornyi, P. M. Ostrovsky, B. Trauzettel, A. D. Mirlin, and M. Titov, Lévy flights due to anisotropic disorder in graphene, Phys. Rev. Lett. **117**, 046603 (2016).
[52] Y.-P. Wang, J. Ren, and C. Fang, Superdiffusive transport on lattices with nodal impurities, Phys. Rev. B **110**, 144201 (2024).
[53] Y.-P. Wang, C. Fang, and J. Ren, Superdiffusive transport in quasi-particle dephasing models, SciPost Phys. **17**, 150 (2024).
[54] Y.-P. Wang, J. Ren, S. Gopalakrishnan, and R. Vasseur, Superdiffusive transport in chaotic quantum systems with nodal interactions, arXiv:2501.08381.
[55] M. Szyniszewski, I. Poboiko, C. Turner, I. Gornyi, A. Mirlin, and A. Pal, Data for "Measurement-induced Lévy flights of quantum information", 2025, 10.25446/oxford.28355921.v1.